Supporting Information

Piatkov et al. 10.1073/pnas.1207786109

SI Results

Proapoptotic Protein Fragments Examined. Descriptions below are the more detailed counterparts (with citations of relevant studies) of the brief descriptions in the text of the 10 previously identified proapoptotic C-terminal protein fragments (Cys-RIPK1, Cys-TRAF1, Asp-BRCA1, Leu-LIMK1, Tyr-NEDD9, Arg-BID, Asp-BCL_{XL}, Arg-BIM_{EL}, Asp-EPHA4, and Tyr-MET) produced by caspases (eight fragments) or calpains (two fragments). These fragments have been shown, in the present work, to be short-lived substrates of the Arg/N-end rule pathway (Figs. 2–4 and Figs. S1 and S2). The fragments are cited in the order of their placements in Figs. 2 and 3. Molecular masses of these proteins were ∼1 kDa larger than their natural sizes (indicated in Figs. 2 and 3 and below), because the fragments contained the ∼1 kDa C-terminal flag epitope. The names of proteins are in capital letters for both human and mouse proteins to make it easy to distinguish these names from the three-letter notations of N-terminal residues. The residue numbers of N-terminal residues in the names of cited fragments are either of mouse or human versions of these proteins, as indicated, and are identical to notations in Figs. 2 and 3.

Cys^{326}-RIPK1. RIPK1 is a conditionally short-lived 77-kDa Ser/Thr kinase and multifunctional regulator of apoptosis, programmed necrosis (necroptosis), and other processes, including antiviral responses that do not involve cell death (refs. 1–11 and references therein). Mouse Cys^{326}-RIPK1 (its human counterpart is Cys^{325}-RIPK1) is the previously identified, caspase-generated, proapoptotic 41-kDa C-terminal fragment of RIPK1. This fragment is proapoptotic at least in part through its facilitation of the activation of caspase-8, which cleaves full-length RIPK1 to generate more Cys-RIPK1. The result is a positive feedback that promotes apoptosis (1–3). The previously shown proapoptotic activity of the Cys-RIPK1 fragment, in the context of circuits that mediate and regulate other activities of RIPK1 (1–6, 11), remains to be understood in mechanistic detail. The Cys-RIPK1 fragment bears N-terminal Cys, a tertiary destabilizing residue (Fig. 1*A*), and it has been shown here to be a short-lived substrate of the Arg/N-end rule pathway (the text, Figs. 2 *B* and *C* and 3*K* and Figs. S1, S2*A*, and S3 *A* and *B*).

Cys^{157}-TRAF1. TRAF1, in conjunction with RIPK1, TRAF2, and other TNF receptor-associated proteins, functions to minimize the activation of caspase-8 and other proapoptotic reactions in part by contributing to the up-regulation of the antiapoptotic NF-κB regulon (5, 12). In contrast to full-length TRAF1, its previously identified caspase-generated Cys-TRAF1 fragment (Cys^{157}-TRAF1 in the case of mouse TRAF1) is proapoptotic, at least in part because it inhibits the activation of NF-κB (12, 13). The Cys-TRAF1 fragment bears N-terminal Cys, a tertiary destabilizing residue, and has been shown here to be a short-lived substrate of the Arg/N-end rule pathway (the text, Figs. 2 *D* and *E* and 3*L*, and Figs. S2*B*).

Asp^{1119}-BRCA1. Mouse BRCA1 (breast cancer suppressor protein-1) is a 199-kDa RING-type E3 ubiquitin ligase (human BRCA1 is a 220-kDa protein) that functions as a tumor suppressor and participates in DNA repair, cell-cycle checkpoint regulation, transcriptional control, centrosome function, X-chromosome inactivation, and other processes as well (refs. 14–16 and references therein). Mouse Asp^{1119}-BRCA1 (its human counterpart is Asp^{1156}-BRCA1) is the previously identified, caspase-generated, proapoptotic 78-kDa C-terminal fragment of BRCA1 that bears N-terminal Asp, a secondary destabilizing residue (Fig. 1*A* and Figs. S1 and S2*C*) (17–19). Ectopic expression of the Asp-BRCA1 fragment (in contrast to a similar expression of full-length BRCA1) can either make cells hypersensitive to apoptosis induced by a variety of agents or cause apoptosis directly, depending on the cell type and conditions of Asp-BRCA1 expression (17–19). In contrast to full-length BRCA1, which is largely nuclear under normal conditions, the Asp-BRCA1 fragment is largely cytosolic (19). The mechanism of proapoptotic activity of the Asp-BRCA1 fragment is unknown. Asp-BRCA1 has been shown here to be a short-lived substrate of the Arg/N-end rule pathway (the text, Figs. 2 *F* and *G* and 4 *C*–*F*, and Fig. S2*C*).

Leu^{241}-LIMK1. Human LIMK1 (LIM kinase-1) is a 73-kDa Ser/Thr kinase that functions, in particular, as a downstream effector of ρ-signaling pathways and regulator of actin dynamic. Among phosphorylation targets of LIMK1 are actin-binding proteins such as cofilin (refs. 20–22 and references therein). Leu^{241}-LIMK1 is the previously identified, caspase-generated, 48-kDa proapoptotic C-terminal fragment of human LIMK1 that contains the active kinase domain and lacks the N-terminal autoinhibitory domain (21). Although it is likely that the proapoptotic activity of the Leu-LIMK1 fragment stems from its increased kinase activity, compared with full-length LIMK1 (21), detailed understanding of proapoptotic effects of Leu-LIMK1 remains to be attained. The Leu-LIMK1 fragment bears N-terminal Leu, a primary destabilizing residue (Fig. 1*A*), and it has been showed here to be a short-lived substrate of the Arg/N-end rule pathway (the text, Figs. 2 *H* and *I*, and Figs. S1 and S2*F*).

Tyr^{631}-NEDD9. Human NEDD9 (neural precursor cell-expressed, developmentally down-regulated 9; one of its other names is human enhancer of filamentation 1) is a 93-kDa scaffolding protein with functions that include cell attachment, migration, and mitotic control. NEDD9 is frequently overexpressed in human cancers, including glioblastomas and breast cancers. NEDD9 is a member of the Cas family that also includes p130CAS and EFS/SIN (refs. 23–27 and references therein). Human Tyr^{631}-NEDD9 is the previously identified, caspase-generated, proapoptotic 24-kDa C-terminal fragment of NEDD9 (23–25). Detailed understanding of proapoptotic effects of Tyr-NEDD9 remains to be attained. The Tyr-NEDD9 fragment is produced largely (possibly exclusively) during apoptosis, bears N-terminal Tyr (a primary destabilizing residue), and has been shown here to be a short-lived substrate of the Arg/N-end rule pathway (the text, Figs. 1*A* and 2 *J* and *K*, and Figs. S1 and S2*E*).

Arg^{71}-BID. Human BID is a 22-kDa member of the BCL-2 family of proteins that regulates the permeabilization of the outer mitochondrial membrane, a step that leads to the release of cytochrome *c* into the cytosol and thereby, initiates apoptosis (5, 28, 29). Although full-length BID is a proapoptotic regulator, its C-terminal fragments, which can be naturally produced by activated caspases, calpains, granzyme B, or cathepsins, can be even more active than intact BID as proapoptotic proteins (30). The cleavage of human BID by activated calpain-1 produces the 14-kDa Arg^{71}-BID proapoptotic fragment (30–33) that has been shown here to be a short-lived substrate of the Arg/N-end rule pathway (Figs. 1*A* and 3 *A* and *B* and Figs. S1 and S2*D*). (The cleavages of BID by caspases produce C-terminal fragments that bear either N-terminal Gly or N-terminal Ser [i.e., the residues

that are not recognized by the Arg/N-end rule pathway (29, 30)].) BID is cleaved by activated calpains during cell death that is induced by cisplatin (a DNA-damaging agent), under conditions that cause endoplasmic reticulum (ER) stress, or in cardiomyocytes during ischemia/reperfusion (30–33). Specific reasons for the observed higher proapoptotic activity of the Arg-BID fragment compared with full-length BID are unknown.

Asp^{61}-BCL$_{XL}$. Mouse BCL$_{XL}$ is a 26-kDa antiapoptotic regulatory protein (5, 34). Under conditions that include glucose and oxygen deprivation of mammalian cells, BCL$_{XL}$ can be cleaved by activated calpain-1, resulting in the 21-kDa Asp^{61}-BCL$_{XL}$ fragment that has proapoptotic activity in contrast to full-length BCL$_{XL}$ (35). The mechanism of proapoptotic activity of the Asp-BCL$_{XL}$ fragment is unknown. Asp-BCL$_{XL}$ bears N-terminal Asp, a secondary destabilizing residue, and it has been shown here to be a short-lived substrate of the Arg/N-end rule pathway (the text, Figs. 1*A* and 3 *C* and *D*, and Figs. S1 and S2*G*).

Arg^{14}-BIM$_{EL}$. Isoforms of BIM (BIM$_{EL}$, BIM$_L$, and BIM$_S$), produced by alternative splicing of *BIM* pre-mRNA, are members of the Bcl-2 family of apoptosis regulators that control, in particular, the mitochondrial permeability transition that results in the release of cytochrome *c* and downstream proapoptotic steps (5). A major function of BIM proteins is to promote the initiation of apoptosis through interactions with mitochondria-associated antiapoptotic Bcl-2–type proteins. Activity of the *BIM* gene plays a role in the development of B and T lymphocytes, and it is required for the physiologically relevant apoptosis of activated T lymphocytes (5, 36, 37). BIM$_{EL}$, a 22 kDa protein, is the major isoform of BIM in T cells. It has been shown that human BIM$_{EL}$ is cleaved by caspase-3 or other caspases during apoptosis, resulting in the 21-kDa Arg^{14}-BIM$_{EL}$ fragment. The proapoptotic activity of Arg^{14}-BIM$_{EL}$ is considerably higher than the activity of uncleaved BIM$_{EL}$ (37). In unperturbed cells, a large fraction of BIM$_{EL}$ dynamically interacts with tubulin of the microtubules, in contrast to BIM$_L$ and BIM$_S$, which do not interact with tubulin. Unphosphorylated BIM$_{EL}$ binds to microtubules, whereas phosphorylated BIM$_{EL}$ has a much lower affinity for them. The tubulin-associated BIM$_{EL}$ is prevented from exerting proapoptotic effects on prosurvival members of the Bcl-2 protein family. During the initiation of apoptosis, BIM$_{EL}$ that dissociates from microtubules is cleaved by caspase-3 or other caspases at the Asp^{13}-Arg^{14} peptide bond. The resulting Arg^{14}-BIM$_{EL}$ fragment has a higher affinity for the prosurvival Bcl-2 protein than the uncleaved, full-length BIM$_{EL}$, thus accounting, at least in part, for the higher proapoptotic activity of caspase-processed Arg^{14}-BIM$_{EL}$ (37). The Arg-BIM$_{EL}$ fragment bears N-terminal Arg, a primary destabilizing residue, and has been shown here to be a short-lived substrate of the Arg/N-end rule pathway (the text, Figs. 1*A* and 3 *E* and *F*, and Fig. S2*H*).

Asp^{774}-EPHA4. Mouse EPHA4 (ephrin receptor A4) is a 110-kDa transmembrane receptor for its ligand EPHRINB3. EPHA4 is a member of the family of more than 10 mammalian dependence receptors (DpRs) (refs. 38–45 and references therein). These DpR receptors are usually not related by sequence or structure but are functionally analogous because of their ability to mediate two opposite physiological outcomes. In the presence of its cognate ligand, a DpR receptor activates signaling pathways that mediate cell survival, migration, proliferation, or differentiation. In the absence of its ligand, a DpR produces a proapoptotic signal, often through the formation, by caspases or other nonprocessive proteases, of a C-terminal proapoptotic fragment that functions in the cytosol and/or the nucleus (38–44). Among the functions of the uncleaved, full-length EPHA4 (in the presence of its cognate ligand EPHRINB3) are the promotion and regulation of neurogenesis. In the absence of EPHRINB3, the intracellular domain of EPHA4 is cleaved by caspase-3 or related caspases, generating the proapoptotic Asp^{774}-EPHA4 fragment (42, 45). The mechanism of proapoptotic activity of the Asp-EPHA4 fragment is unknown. This 24-kDa fragment bears N-terminal Asp, a secondary destabilizing residue, and it has been shown here to be a short-lived substrate of the Arg/N-end rule pathway (the text, Figs. 1*A* and 3 *G* and *H*, and Figs. S1 and S2*I*).

Tyr^{1001}-MET. The mouse transmembrane receptor MET (its other name is hepatocyte growth factor receptor) is the second dependence receptor (other than EPHA4) examined in the present work. MET is a 154-kDa receptor tyrosine kinase with functions in embryonic development and organ formation (refs. 38–42 and 46–50 and references therein). In the absence of its cognate ligand, such as the 80-kDa hepatocyte growth factor, the intracellular domain of MET is cleaved by caspase-3 or related caspases, generating the proapoptotic 43-kDa Tyr^{1001}-MET fragment [~42 kDa if one takes into account a cleavage at the second, C terminus-proximal caspase cleavage site in mouse MET at Asp^{1374}-Gly^{1375}, five residues upstream of the last (Thr^{1379}) residue of MET] (42, 45, 48–50). The mechanism of proapoptotic activity of Tyr-MET is unknown. The Tyr-MET fragment bears N-terminal Tyr, a secondary destabilizing residue, and it has been shown here to be a short-lived substrate of the Arg/N-end rule pathway (the text, Figs. 1*A* and 3 *I* and *J*, and Figs. S1 and S2*J*).

SI Materials and Methods

Miscellaneous Reagents. Cycloheximide and tamoxifen were from Sigma. Mouse and human cDNAs were from OpenBiosystems. Z-DEVD-FMK and Z-VAD-FMK were from Enzo Life Sciences. The following antibodies were used: anti-FLAG M2 (F1804; Sigma), anti-HA (H3663; Sigma); anti-RIPK1 (a monoclonal antibody to a C-terminal region of human RIPK1 that cross-reacts with mouse Ripk1; 610458; BD Biosciences); anticaspase-3 (9662S; Cell Signaling); anti-BRCA1 (I-20, Sc-646; Santa Cruz); affinity-purified polyclonal antibody to mouse ATE1 (51); and affinity-purified polyclonal antibody to mouse UBR1 (52). The latter antibody was used as a 1:1 mixture of affinity-purified polyclonal antibodies to the synthetic peptides EMDPDLEKQEESVQ (UBR1 residues 54–67) and HEPGRAGTTKESLH (UBR1 residues 166–179), respectively (52). Clean-Blot IP Detection Reagent was from Thermo Scientific (21210). The following reagents were used for immunoprecipitation: anti-FLAG M2 Magnetic Beads (M8823; Sigma), Protein A/G Magnetic Beads (88802; Pierce), and EZview Red anti-HA affinity gel (E6779; Sigma). Recombinant human TNFα was from R&D, Inc. (210-TA) and Shenandoah Biotechnology, Inc. (100-111). Recombinant active human caspase-8 was from Cayman Chemical.

Animal Care and Treatments. All animal care and procedures were carried out according to the relevant National Institutes of Health guidelines, and they were approved (protocol #1328) by the Institutional Animal Care and Use Committee and the Office of Laboratory Animal Research at the California Institute of Technology, where the present study was performed. Mice were housed at ~22 °C using a 12 h light to 12 h dark cycle, with Laboratory Rodent Diet 5001 (PMI International) ad libitum. In conditionally ATE1-deficient *Ate1$^{flox/-}$; CaggCreER* mice, one copy of *Ate1* was inactive, whereas the other (floxed) copy of *Ate1* could be inactivated in adult mice through a transient activation of Cre recombinase, which was expressed from the ubiquitously active chimeric *Cagg* promoter and transiently activated by tamoxifen (53). ATE1-containing mice were *Ate1$^{flox/+}$* and lacked Cre. *Ate1$^{flox/-}$; CaggCreER* and *Ate1$^{flox/+}$* mice between 3 and 8 wk of age were treated with tamoxifen (2 mg in 0.2 mL sesame oil) by daily i.p. injections over 5 d (53); 3 wk after tamoxifen treatment (53), TNFα (50 μg/kg) was administered by

tail vein injection. Specific tissues were harvested and analyzed by immunoblotting 12 h after TNFα injection.

Plasmids, cDNAs, and Primers. DH5α *Escherichia coli* (Invitrogen) was used for cloning and maintaining plasmids. Phusion High-Fidelity DNA polymerase (New England Biolabs) was used for PCR. Sequences of all constructed plasmids were verified by DNA sequencing. The plasmid pKP496 was constructed by ligation of annealed primers 1,447 and 1,448 into SacII/XbaI-cut pcDNA3fDHFRUbR48Xpr (54). The resulting plasmid, which encoded the ^{f}DHFR-Ub^{K48R}-MCS (SacII-EcoRI-XhoI-ClaI-EcoRV)-flag fusion, was used to construct plasmids for the ubiquitin reference technique (55).

RIPK1. The human *RIPK1* ORF was amplified from a human HeLa cDNA library using primers 652, 653, and 647 (Table S2) that encoded a C-terminal ha$_2$-flag epitope. The resulting DNA fragment was inserted into pcDNA3-Neo (Invitrogen) using *Hind*III/XhoI sites. A plasmid expressing mouse *Ripk1* cDNA was produced similarly using a cDNA library from C57BL/6 mice and primers 650, 651, and 647 (Table S2). The plasmids pKP395, pKP396, and pKP397, which expressed flag-DHFR-Ub-X-RIPK1-flag fusions (X = Cys, Asp, Val; mouse RIPK1) were constructed by amplifying the mouse RIPK1-encoding DNA fragment with the following sets of primers: 702, 697, and 706 (Cys^{326}-RIPK1); 703, 697, and 706 (Asp^{326}-RIPK1); and 705, 697, and 706 (Val^{326}-RIPK1). The resulting fragments were digested with SmaI and XbaI and were cloned into *Sfo*I/XbaI-cut pcDNA3fDHFRUbR48Xpr (54). The pcDNA5/FRT/TO plasmid (Invitrogen) containing a tetracycline-regulated, hybrid human cytomegalovirus *CMV/TetO2* promoter was used to construct the plasmids pcDNA5/TO/Ub-X^{325}-RIPK1, which encoded Ub^{R48}-X^{325}-RIPK^{f} (human RIPK1); x was a variable residue at the Ub–protein junction (55). These plasmids were constructed by ligating PCR-produced DNA fragments to XhoI/XbaI-cut pcDNA5/FRT/TO.

TRAF1. The mouse *Traf1* ORF was amplified using cDNA from OpenBiosystems (30748947) and primers 1,188 and 1,189. The resulting fragment was cut with *BamH*I and XbaI and cloned into *BamH*I/XbaI-cut pcDNA3.0 (Invitrogen), generating the plasmid pKP378. The ORF of mouse *Traf1* containing the D156A point mutation was amplified using primers 1,188, 1,190, 1,191, 1,189, and pKP378 (Table S2) as a template. The resulting fragment was cut with *BamH*I and XbaI and cloned into *BamH*I/XbaI-cut pcDNA3.0 (Invitrogen), generating the plasmid pKP379. The plasmids pKP380, pKP381, and pKP382, which expressed flag-Ub-X^{157}-TRAF^{f} fusions (X = Cys, Asp, Val; mouse Traf1), were constructed by amplifying the mouse TRAF1-encoding DNA fragment with the following sets of primers: 1,192 and 1,189 (Cys^{157}-TRAF1); 1,195 and 1,189 (Asp^{157}-TRAF1); and 1,196 and 1,189 (Val^{157}-TRAF1). The resulting fragments were linked to DNA encoding flag-tagged Ub (constructed by PCR amplification using primers 1,197, 1,198, 1,194, and the pcDNA3fDHFRUbR48Xpr plasmid as a template) using primers 1,197 and 1,189. The resulting DNA fragment was cut with *BamH*I and XbaI and cloned into *BamH*I/XbaI-cut pcDNA3fDHFRUbR48Xpr (54).

BRCA1. The mouse *Brca1* ORF was amplified using cDNA from OpenBiosystems (30431022) and primers 1,438 and 1,440 for Asp^{1119}-BRCA1 or 1,439 and 1,440 (Table S2) for Val^{1119}-BRCA1. The resulting DNA fragments were cut with SacII and ClaI and cloned into SacII/ClaI-cut pKP496, generating the plasmids pKP528 and pKP529, respectively.

LIMK1. The human *LIMK1* ORF was amplified using cDNA from OpenBiosystems (LIFESEQ95191844) and primers 1,467 and 1,469 for Leu^{241}-LIMK1 or 1,468 and 1,469 for Val^{241}-LIMK1. The resulting fragments were cut with SacII and ClaI and cloned into SacII/ClaI-cut pKP496, generating the plasmids pKP512 and pKP513, respectively.

NEDD9. The human *NEDD9* ORF was amplified using cDNA from OpenBiosystems (6299616) and primers 1,479 and 1,481 for Tyr^{631}-NEDD9 or 1,480 and 1,481 for Val^{631}-NEDD9. The resulting fragments were cut with SacII and ClaI and cloned into SacII/ClaI-cut pKP496, generating the plasmids pKP526 and pKP527, respectively.

BID. The human *BID* ORF was amplified using cDNA from OpenBiosystems (5179075) and primers 1,473 and 1,475 for Arg^{71}-BID or 1,474 and 1,475 Val^{71}-BID. The resulting fragments were digested with SacII and ClaI and cloned into SacII/ClaI-cut pKP496, generating the plasmids pKP523 and pKP524, respectively.

BCL$_{XL}$. The mouse *Bcl$_{XL}$* ORF was amplified using cDNA from OpenBiosystems (6830063) and primers 1,432 and 1,434 for Asp^{61}-BCL$_{XL}$ or 1,433 and 1,434 for Val^{61}-BCL$_{XL}$. The resulting fragments were cut with SacII and ClaI and cloned into SacII/ClaI-cut pKP496, generating the plasmids pKP514 and pKP515, respectively.

BIM$_{EL}$. The mouse *Bim$_{EL}$* ORF was amplified using cDNA from OpenBiosystems (4459720) and primers 1,435 and 1,437 for Arg^{14}-BIM$_{EL}$ or 1,436 and 1,437 for Val^{14}-BIM$_{EL}$. The resulting fragments were cut with SacII and ClaI and cloned into SacII/ClaI-cut pKP496, generating the plasmids pKP521 and pKP522, respectively.

EPHA4. The mouse *EphA4* ORF was amplified using cDNA from OpenBiosystems (IMAGE 6512978) and primers 1,369 and 1,371 for Asp^{774}-EPHA4 or 1,427 and 1,428 for Val^{774}-mEPHA4. The resulting fragments were cut with SmaI and XbaI and cloned into *Sfo*I/XbaI-cut pcDNA3fDHFRUbR48Xpr, generating the plasmids pKP492 and pKP493, respectively.

MET. The mouse *MET* was amplified using cDNA from OpenBiosystems (IMAGE 40098362) and primers 1,426 and 1,428 for Tyr^{1001}-MET or 1,427 and 1,428 for Val^{1001}-MET. The resulting fragments were cut with SacII and ClaI and cloned into SacII/ClaI-cut pKP496, generating the plasmids pKP519 and pKP520, respectively.

Tissue Extracts and Immunoblotting. Mouse tissues were processed in Triton lysis buffer (1% Triton X-100, 50 mM NaCl, 2 mM EDTA, 50 mM Tris·HCl, pH 7.4) containing complete protease inhibitor cocktail (Roche) using the MP FastPrep-24 instrument and Lysing Matrix D (MP Biomedicals), with three runs at 6.5 m/s for 20 s each and 5-min incubations on ice between the runs. The extracts were centrifuged at 10,000 × g for 10 min at 4 °C. Total protein concentrations in the supernatants were determined using the BCA assay (Pierce), followed by the addition of a concentrated SDS sample buffer (to the final concentration of 1× SDS sample buffer), heating at 95 °C for 10 min, and SDS 4–15% PAGE, with 100 μg total protein per lane. Fractionated proteins were analyzed by immunoblotting (including electroblotting to Immobilon-P PVDF membranes; Millipore) using antibodies indicated. Immunoblots were visualized using SuperSignal West Pico or SuperSignal West Femto reagents (Thermo Scientific) or ECL Plus Western blotting Detection System (GE Healthcare) according to manufacturer's instructions.

TUNEL Assays with Mouse Tissues. Recombinant human TNFα (50 μg/kg body weight) dissolved in PBS containing 0.2% BSA was injected into the tail vein of ~2-mo-old mice 3 wk after tamox-

ifen treatment to induce ablation of the floxed *Ate1* gene (in the text and ref. 53); 12 h after TNFα injection, mice were anesthetized by an i.p. injection of Na-pentobarbital (40 mg/kg; Nembutal; Abbott Laboratories), and their organs were fixed with 4% formaldehyde in PBS by cardiac perfusion. Thereafter, specific tissues were removed and embedded with paraffin using standard procedures. After sectioning into 10-μm sections, tissues were assayed using the fluorescein-based In Situ Cell Death Detection Kit (Roche) according to the manufacturer's protocol. The sections were then counterstained with DAPI and analyzed by fluorescence microscopy using a Zeiss Axiophot microscope.

Cell Cultures and Apoptosis Assays. The mouse NIH-3T3 cell line was from American Type Culture Collection and grown in the DMEM supplemented with 10% FBS (Gibco) and penicillin/streptomycin (100 units/mL; HyClone). Human Flp-In T-REx-293 cells (Invitrogen) were grown similarly, but DMEM was supplemented with tetracycline-free 10% FBS (Tet-free FBS; Clontech). T-REx-293–based human cell lines expressing Ub-X-RIPK1 fusions (X = Cys, Asp, Val; in the text) from a doxycycline (Dox) -inducible promoter were produced using an Flp recombinase-mediated integration system in these cells (Invitrogen). Briefly, pcDNA5/FRT/TO (vector alone), pKP418, pKP419, or pKP420 (Table S1) were cotransfected with pOG44 (transiently expressing Flp recombinase) into T-REx-293 cells using Lipofectamine-2000 (Invitrogen); 48 h posttransfection, each transfected cell culture was split in one-half and plated in the presence of hygromycin B (100 μg/mL; Invitrogen). After 2–3 wk, individual cell colonies were isolated and analyzed by immunoblotting to detect a Dox-dependent expression of a transgene.

Untransformed primary (precrisis) mouse embryonic fibroblasts (EFs) were prepared using previously described techniques (56). These primary EFs were derived from the previously described ATE1-containing *Ate1*$^{flox/-}$, CreER E15 embryos that were heterozygous at the *Ate1* locus (53). Two recently and equally split cultures of *Ate1*$^{flox/-}$, CreER primary EF cells were treated daily with either 50 nM tamoxifen in DMSO (to ablate the floxed *Ate1* allele) or DMSO alone for 5 consecutive d. Both control and experimental cultures were grown in the absence of DMSO/tamoxifen for an additional 7 d. Thereafter, the cultures were treated for 24 h with increasing concentrations of TNFα (between 0 and 25 ng/mL) in DMEM that also contained 0.5% FBS and a nontoxic (2.5 μg/mL) concentration of cycloheximide. In most experiments, 10^6 cells/well were treated in a 24-well plate for indicated times. Cells were then washed on a plate one time with PBS, lysed in 1% SDS supplemented with protease inhibitors, and heated at 95 °C for 5 min. Protein concentration in the samples was determined using the BCA assay (Pierce). One volume of 2× SDS sample buffer was added, the resulting samples were heated at 95 °C for 5 min, and 50 μg protein per lane were fractionated by SDS 4–15% PAGE, followed by immunoblotting with a monoclonal antibody to a C-terminal region of RIPK1 or an affinity-purified antibody to mouse ATE1. All immunoblots were also analyzed for sample-loading uniformity using antitubulin antibody as well as staining of proteins with Coomassie-R250.

Colony-formation assays were carried out with WT, *Ate1*$^{-/-}$, and *Ubr1*$^{-/-}$ *Ubr2*$^{-/-}$ double-mutant EF cell lines. These EF cell lines were produced and characterized previously (52, 57–59). For experiments in the present study, we used *Ubr1*$^{-/-}$ *Ubr2*$^{-/-}$ EFs (58, 59) and also, an *Ate1*$^{-/-}$ EF cell line (as well as its WT EF counterpart) that was produced using previously described methods (57) but independently and specifically in the present work using E13.5 *Ate1*$^{-/-}$ embryos and their WT littermates.

For TUNEL analysis of EF cell lines or primary (precrisis) EF cells in culture, cells were grown in DMEM (Gibco) supplemented with 10% FBS, standard antibiotics, and 2 mM L-glutamine. Cells were plated at ∼0.5 × 10^5 cells per 22-mm well on coverslips coated with poly-L-lysine. After 12 h, cells were treated with increasing concentrations of staurosporine (between 0 and 1 μM) for 24 h or specified doses of ∼260 nm UV irradiation followed by fixation in 4% formaldehyde. Cells were then analyzed using TUNEL as described above.

Assay for Activated Caspase-3. Caspase activity was measured using the fluorogenic substrate Ac-DEVD-AMC (Caspase-3 Assay Kit; Pharmingen) according to the manufacturer's protocol. Briefly, T-Rex-293–based cell cultures, at 80–90% confluence, were treated with trypsin to detach the cells and stained with Trypan Blue (to measure the percentage of dead cells); total cell numbers were determined using a hemocytometer. Cells were seeded into a 96-well plate with 10^4 cells/well containing 0.1 mL DMEM and 10% FBS, and they were incubated for 24 h with increasing concentrations of Dox. Then, cells were incubated for another 12 h with cycloheximide (at its nontoxic concentration of 2.5 μg/mL). Thereafter, the medium was removed, and cells were washed one time with PBS; 30 μL buffer A (10 mM KCl, 1.5 mM $MgCl_2$, 1 mM EDTA, 1 mM EGTA, 1 mM DTT, 0.1 mM PMSF, 20 mM Hepes, pH 7.2) containing complete protease-inhibitor mixture (Roche) were added to each well, and the plate was incubated on ice for 20 min followed by breaking the cells through three cycles of freezing in liquid N_2 and thawing the samples at 37 °C in a water bath. The resulting samples were centrifuged at 3,000 × g for 30 min. Protein concentrations in the supernatants were determined using Coomassie Plus Protein Assay (Pierce). Centrifugation-clarified extracts (20 μg total protein) were incubated with 5 μg Ac-DEVD-AMC, a fluorogenic caspase-3 substrate, in the total volume of 0.2 mL at 37 °C for 1 h followed by measurements of fluorescence in a microplate fluorimeter using 380-nm excitation and 430-nm emission filters.

In Vitro Caspase Assays with ATE1 and UBR1. Purified Ate1^{1B7A} isoform of the Ate1 R-transferase (60, 61) or an extract from NIH-3T3 cells was incubated with active recombinant human caspase-8 followed by SDS 4–12% PAGE and immunoblotting with affinity-purified antibodies to mouse ATE1 or mouse UBR1.

In Vitro Transcription–Translation–Degradation Assay. The TNT T7 Coupled Transcription/Translation System, a version of the Promega rabbit reticulocyte extract preparation in which the main components of the system were supplied separately, was used to carry out transcription–translation–degradation assays. Reaction samples were prepared according to the manufacturer's instructions. Newly formed proteins in reticulocyte extract were pulse-labeled with L-[^{35}S]methionine (0.55 mCi/mL, 1,000 Ci/mmol; MP Biomedicals) for 5 min in total volume of 30 μL. The labeling was quenched by the addition of cycloheximide and unlabeled methionine to the final concentrations of 0.1 mg/mL and 5 mM, respectively. Unless stated otherwise, the reactions were carried out at 30 °C and terminated by the addition of an equal volume of TDS (Tris-dodecyl-sulfate) buffer (1% SDS, 5 mM DTT, 50 mM Tris·HCl, pH 7.4, also containing complete protease-inhibitor mixture; Roche) followed by heating at 95 °C for 10 min. The resulting samples were diluted with 10 volumes of TNN (Tris-Nonidet-NaCl) buffer (0.5% Nonidet P-40, 0.25 M NaCl, 5 mM EDTA, 50 mM Tris·HCl, pH 7.4, also containing complete protease-inhibitor mixture; Roche), and the amounts of ^{35}S in the 10% CCl_3COOH-insoluble fraction were measured. For immunoprecipitation, samples were adjusted to contain equal amounts of total ^{35}S and were added to 10 μL beads with an immobilized antibody, either antiflag or antiha (see above). The samples were incubated with rocking at 4 °C for 4 h, followed by four washes in TNN buffer, resuspension in 20 μL SDS sample buffer, and heating at 95 °C for 10 min followed by SDS 4–15% PAGE and autoradiography. Quantification of autoradiograms was carried out using PhosphorImager (Molecular Dynamics).

Alternatively, the samples (not labeled with ^{35}S) were analyzed using immunoblotting with indicated antibodies.

In Vitro Arginylation Assay. The arginyl-transferase (R-transferase) assay (20 μL) contained an extract from NIH 3T3 cells (4 mg/mL total protein), α-lactalbumin (arginylation reporter; 1.25 mg/mL) (60), total *E. coli* tRNA (0.6 mg/mL; Sigma), total *E. coli* aminoacyl-tRNA synthetases (800 U/mL; Sigma), 5 μM MG132 (proteasome inhibitor; Sigma), 2 mM ATP, 0.15 M KCl, 10 mM $MgCl_2$, 1 mM DTT, 50 mM Tris·HCl (pH 8.0), 10 mM phosphocreatine, creatine kinase (20 μg/mL; Sigma), 2 μM Arg, and 0.3 μM L-^{3}H-arginine (PerkinElmer). The reaction mixture was incubated for 60 min at 30 °C and deposited onto Whatman 3MM filter disks (GE Healthcare). The filters were incubated for 10 min in 10% cold CCl_3COOH, followed by 10 min in 10% CCl_3COOH at 95 °C. The filters were then washed in 5% CCl_3COOH three times at room temperature followed by a single diethyl ether-ethanol (1:1) wash, two diethyl ether washes, and measurements of ^{3}H retained on a filter using a scintillation spectrometer. The R-transferase assay for ATE1 that had been treated with caspase-8 was performed identically, except that L-^{14}C-arginine was used. The reaction mixture was incubated for 60 min at 30 °C. The reaction was terminated by the addition of an equal volume of 2× SDS sample buffer and heating at 95 °C for 10 min, followed by SDS 4–15% PAGE and autoradiography.

Antibody Specific for Arg-Asp^{1119}-BRCA1, the Nt-Arginylated Asp^{1119}-BRCA1 Fragment. Rabbit peptide-mediated antibody to **R**DVEIQGHTSFC, the Nt-arginylated N-terminal sequence of the Asp^{1119}-BRCA1 fragment (except for C-terminal Cys, which was used to conjugate the peptide to a carrier protein) was produced by Abgent using standard methods. The peptides **R**DVEIQGHTSFC and its nonarginylated counterpart DVEIQGHTSFC were synthesized and purified also by Abgent. The resulting antibody was affinity-purified at first positively against the immobilized **R**DVEIQGHTSFC peptide using standard methods (62). The peptide-bound antibody fraction was eluted and saved. This fraction was thereafter negatively purified against the immobilized DVEIQGHTSFC peptide. The unbound fraction, used as the antibody to the Nt-arginylated Arg-Asp^{1119}-BRCA1 fragment (Fig. 4*E*), was strikingly specific for the **R**DVEIQGHTSFC peptide (Fig. 4*B*). Immunoblotting was carried out (with the antibody at 0.3 μg/mL) for 8 h at room temperature in 5% skim milk in TBS containing 0.1% Tween-20. The bound antibody was detected using the Chemiluminescent Kit (ECL Plus; GE Healthcare Life Sciences) and a goat anti-rabbit antibody (at 1:2,000 dilution) conjugated to HRP.

Pulse-Chase Assay with Endogenous BRCA1. Mouse EF cell lines were grown in DMEM (Gibco) supplemented with 10% FBS, standard antibiotics, and 2 mM L-glutamine. Cells were plated at ∼70% confluence in 10-cm plates (one plate per each time point). After 12 h, cells were treated with UV irradiation (∼260 nm and 60 J/m^2), followed by incubation for 4 h and the labeling of cells with [^{35}S]methionine/cysteine (1 mCi per plate) for 60 min in DMEM without methionine (Sigma). Caspase inhibitors Z-DEVD-FMK (3 μM) and Z-VAD-FMK (100 μM; a pan-caspase inhibitor) as well as unlabeled methionine and cysteine (to 2 mM) were then added followed by a chase for 1 and 2 h. Plates were washed two times with 1× PBS, and cells were lysed by adding 1 mL TDS$^{0.1}$ buffer (0.1% SDS, 5 mM DTT, 50 mM Tris·HCl, pH 7.4, also containing complete protease-inhibitor mixture; Roche) followed by heating at 95 °C for 10 min. The resulting samples were diluted with 10 volumes TNN$^{0.25}$ buffer (0.25% Nonidet P-40, 0.125 M NaCl, 5 mM EDTA, 50 mM Tris·HCl, pH 7.4, also containing complete protease-inhibitor mixture), and the amounts of ^{35}S in the 10% CCl_3COOH-insoluble fraction of each sample were determined. For immunoprecipitation, samples were adjusted to contain equal amounts of total ^{35}S (∼1×10^8 cpm) and were added to 40 μL anti-BRCA1 antibody (I-20; Santa Cruz). The samples were incubated with rocking at 4 °C for 4 h. Protein A/G Magnetic Beads (Pierce) were then added followed by additional incubation for 1 h at 4 °C. Beads were collected followed by four washes in TNN buffer, resuspension in 20 μL SDS sample buffer, and heating at 95 °C for 10 min, which was followed by SDS 4–12% PAGE and autoradiography. Quantification of autoradiograms was carried out using PhosphorImager (Molecular Dynamics).

1. Lin Y, Devin A, Rodriguez Y, Liu Z-G (1999) Cleavage of the death domain kinase RIP by caspase-8 prompts TNF-induced apoptosis. *Genes Dev* 13:2514–2526.
2. Kim JW, Choi E-J, Joe CO (2000) Activation of death-inducing signaling complex (DISC) by pro-apoptotic C-terminal fragment of RIP. *Oncogene* 19:4491–4499.
3. Martinon F, Holler N, Richard C, Tschopp J (2000) Activation of a pro-apoptotic amplification loop through inhibition of NF-kappaB-dependent survival signals by caspase-mediated inactivation of RIP. *FEBS Lett* 468:134–136.
4. Rajput A, et al. (2011) RIG-I RNA helicase activation of IRF3 transcription factor is negatively regulated by caspase-8-mediated cleavage of the RIP1 protein. *Immunity* 34:340–351.
5. Green DR (2011) *Means to an End: Apoptosis and Other Cell Death Mechanisms* (Cold Spring Harbor Laboratory Press, Plainview, NY).
6. Green DR, Oberst A, Dillon CP, Weinlich R, Salvesen GS (2011) RIPK-dependent necrosis and its regulation by caspases: A mystery in five acts. *Mol Cell* 44:9–16.
7. Oberst A, Green DR (2011) It cuts both ways: Reconciling the dual roles of caspase 8 in cell death and survival. *Nat Rev Mol Cell Biol* 12:757–763.
8. Feoktistova M, et al. (2011) cIAPs block Ripoptosome formation, a RIP1/caspase-8 containing intracellular cell death complex differentially regulated by cFLIP isoforms. *Mol Cell* 43:449–463.
9. Tenev T, et al. (2011) The Ripoptosome, a signaling platform that assembles in response to genotoxic stress and loss of IAPs. *Mol Cell* 43:432–448.
10. Biton S, Ashkenazi A (2011) NEMO and RIP1 control cell fate in response to extensive DNA damage via TNF-α feedforward signaling. *Cell* 145:92–103.
11. Wang L, Du F, Wang X (2008) TNF-alpha induces two distinct caspase-8 activation pathways. *Cell* 133:693–703.
12. Taylor RC, Cullen SP, Martin SJ (2008) Apoptosis: Controlled demolition at the cellular level. *Nat Rev Mol Cell Biol* 9:231–241.
13. Henkler F, et al. (2003) Caspase-mediated cleavage converts the tumor necrosis factor (TNF) receptor-associated factor (TRAF)-1 from a selective modulator of TNF receptor signaling to a general inhibitor of NF-kappaB activation. *J Biol Chem* 278:29216–29230.
14. O'Donovan PJ, Livingston DM (2010) BRCA1 and BRCA2: Breast/ovarian cancer susceptibility gene products and participants in DNA double-strand break repair. *Carcinogenesis* 31:961–967.
15. Pathania S, et al. (2011) BRCA1 is required for postreplication repair after UV-induced DNA damage. *Mol Cell* 44:235–251.
16. Zhu Q, et al. (2011) BRCA1 tumour suppression occurs via heterochromatin-mediated silencing. *Nature* 477:179–184.
17. Zhan Q, et al. (2002) Caspase-3 mediated cleavage of BRCA1 during UV-induced apoptosis. *Oncogene* 21:5335–5345.
18. Sundararajan R, Chen G, Mukherjee C, White E (2005) Caspase-dependent processing activates the proapoptotic activity of deleted in breast cancer-1 during tumor necrosis factor-alpha-mediated death signaling. *Oncogene* 24:4908–4920.
19. Dizin E, Ray H, Suau F, Voeltzel T, Dalla Venezia N (2008) Caspase-dependent BRCA1 cleavage facilitates chemotherapy-induced apoptosis. *Apoptosis* 13:237–246.
20. Nagata K, Ohashi K, Yang N, Mizuno K (1999) The N-terminal LIM domain negatively regulates the kinase activity of LIM-kinase 1. *Biochem J* 343:99–105.
21. Tomiyoshi G, Horita Y, Nishita M, Ohashi K, Mizuno K (2004) Caspase-mediated cleavage and activation of LIM-kinase 1 and its role in apoptotic membrane blebbing. *Genes Cells* 9:591–600.
22. Tapia T, Ottman R, Chakrabarti R (2011) LIM kinase1 modulates function of membrane type matrix metalloproteinase 1: Implication in invasion of prostate cancer cells. *Mol Cancer*, 10.1186/1476-4598-10-6.
23. Law SF, O'Neill GM, Fashena SJ, Einarson MB, Golemis EA (2000) The docking protein HEF1 is an apoptotic mediator at focal adhesion sites. *Mol Cell Biol* 20:5184–5195.
24. O'Neill GM, Golemis EA (2001) Proteolysis of the docking protein HEF1 and implications for focal adhesion dynamics. *Mol Cell Biol* 21:5094–5108.
25. Singh MK, Cowell L, Seo S, O'Neill GM, Golemis EA (2007) Molecular basis for HEF1/NEDD9/Cas-L action as a multifunctional co-ordinator of invasion, apoptosis and cell cycle. *Cell Biochem Biophys* 48:54–72.
26. Tikhmyanova N, Golemis EA (2011) NEDD9 and BCAR1 negatively regulate E-cadherin membrane localization, and promote E-cadherin degradation. *PLoS One* 6:e22102.
27. Kong C, et al. (2011) NEDD9 is a positive regulator of epithelial-mesenchymal transition and promotes invasion in aggressive breast cancer. *PLoS One* 6:e22666.
28. Yin X-M (2006) Bid, a BH3-only multifunctional molecule, is at the cross road of life and death. *Genes Cells* 369:7–19.

29. Billen LP, Shamas-Din A, Andrews DW (2008) Bid: A Bax-like BH3 protein. *Oncogene* 27(Suppl 1):S93–S104.
30. Chen M, et al. (2001) Bid is cleaved by calpain to an active fragment in vitro and during myocardial ischemia/reperfusion. *J Biol Chem* 276:30724–30728.
31. Mandic A, et al. (2002) Calpain-mediated Bid cleavage and calpain-independent Bak modulation: Two separate pathways in cisplatin-induced apoptosis. *Mol Cell Biol* 22: 3003–3013.
32. Gil-Parrado S, et al. (2002) Ionomycin-activated calpain triggers apoptosis. A probable role for Bcl-2 family members. *J Biol Chem* 277:27217–27226.
33. Cabon L, et al. (2012) BID regulates AIF-mediated caspase-independent necroptosis by promoting BAX activation. *Cell Death Differ* 19:245–256.
34. García-Sáez AJ, Ries J, Orzáez M, Pérez-Payà E, Schwille P (2009) Membrane promotes tBID interaction with BCL(XL). *Nat Struct Mol Biol* 16:1178–1185.
35. Nakagawa T, Yuan J (2000) Cross-talk between two cysteine protease families. Activation of caspase-12 by calpain in apoptosis. *J Cell Biol* 150:887–894.
36. Strasser A, Cory S, Adams JM (2011) Deciphering the rules of programmed cell death to improve therapy of cancer and other diseases. *EMBO J* 30:3667–3683.
37. Chen DZ, Zhou Q (2004) Caspase cleavage of Bim_{EL} triggers a positive feedback amplification of apoptotic signaling. *Proc Natl Acad Sci USA* 101:1235–1240.
38. Mehlen P, Thibert C (2004) Dependence receptors: Between life and death. *Cell Mol Life Sci* 61:1854–1866.
39. Porter AG, Dhakshinamoorthy S (2004) Apoptosis initiated by dependence receptors: A new paradigm for cell death? *Bioessays* 26:656–664.
40. Stupack DG (2005) Integrins as a distinct subtype of dependence receptors. *Cell Death Differ* 12:1021–1030.
41. Ancot F, Foveau B, Lefebvre J, Leroy C, Tulasne D (2009) Proteolytic cleavages give receptor tyrosine kinases the gift of ubiquity. *Oncogene* 28:2185–2195.
42. Goldschneider D, Mehlen P (2010) Dependence receptors: A new paradigm in cell signaling and cancer therapy. *Oncogene* 29:1865–1882.
43. Mehlen P, Guenebeaud C (2010) Netrin-1 and its dependence receptors as original targets for cancer therapy. *Curr Opin Oncol* 22:46–54.
44. Thibert C, Fombonne J (2010) Dependence receptors: Mechanisms of an announced death. *Cell Cycle* 9:2085–2091.
45. Furne C, et al. (2009) EphrinB3 is an anti-apoptotic ligand that inhibits the dependence receptor functions of EphA4 receptors during adult neurogenesis. *Biochim Biophys Acta* 1793:231–238.
46. Jones, DSI, 2nd, Tsai P-C, Cochran JR (2011) Engineering hepatocyte growth factor fragments with high stability and activity as Met receptor agonists and antagonists. *Proc Natl Acad Sci USA* 108:13035–13040.
47. Clague MJ (2011) Met receptor: A moving target. *Sci Signal* 4:pe40.
48. Tulasne D, et al. (2004) Proapoptotic function of the MET tyrosine kinase receptor through caspase cleavage. *Mol Cell Biol* 24:10328–10339.
49. Foveau B, et al. (2007) Amplification of apoptosis through sequential caspase cleavage of the MET tyrosine kinase receptor. *Cell Death Differ* 14:752–764.
50. Tulasne D, Foveau B (2008) The shadow of death on the MET tyrosine kinase receptor. *Cell Death Differ* 15:427–434.
51. Hu R-G, et al. (2005) The N-end rule pathway as a nitric oxide sensor controlling the levels of multiple regulators. *Nature* 437:981–986.
52. Kwon YT, Xia Z, Davydov IV, Lecker SH, Varshavsky A (2001) Construction and analysis of mouse strains lacking the ubiquitin ligase UBR1 (E3alpha) of the N-end rule pathway. *Mol Cell Biol* 21:8007–8021.
53. Brower CS, Varshavsky A (2009) Ablation of arginylation in the mouse N-end rule pathway: Loss of fat, higher metabolic rate, damaged spermatogenesis, and neurological perturbations. *PLoS One* 4:e7757.
54. Sheng J, Kumagai A, Dunphy WG, Varshavsky A (2002) Dissection of c-MOS degron. *EMBO J* 21:6061–6071.
55. Varshavsky A (2005) Ubiquitin fusion technique and related methods. *Methods Enzymol* 399:777–799.
56. Robertson EJ (1987) Embryo-derived stem cell lines. *Teratocarcinomas and Embryonic Stem Cells: A Practical Approach*, ed Robertson EJ (IRL, Oxford), pp 71–112.
57. Kwon YT, et al. (2002) An essential role of N-terminal arginylation in cardiovascular development. *Science* 297:96–99.
58. Tasaki T, et al. (2005) A family of mammalian E3 ubiquitin ligases that contain the UBR box motif and recognize N-degrons. *Mol Cell Biol* 25:7120–7136.
59. An JY, et al. (2006) Impaired neurogenesis and cardiovascular development in mice lacking the E3 ubiquitin ligases UBR1 and UBR2 of the N-end rule pathway. *Proc Natl Acad Sci USA* 103:6212–6217.
60. Hu R-G, et al. (2006) Arginyltransferase, its specificity, putative substrates, bidirectional promoter, and splicing-derived isoforms. *J Biol Chem* 281:32559–32573.
61. Hu R-G, Wang H, Xia Z, Varshavsky A (2008) The N-end rule pathway is a sensor of heme. *Proc Natl Acad Sci USA* 105:76–81.
62. Ausubel FM, et al. (2010) *Current Protocols in Molecular Biology* (Wiley Interscience, New York).

Protein	Cleavage site	Nt-residue	C-terminal fragment
Proapoptotic protein fragments that are experimentally confirmed N-end rule substrates			
Mm **RIPK1**	321 SLQHD↓**C**VPL...S 656	Nd^t	Proapoptotic fragment, generated by caspase-8, of the RIPK1 kinase. Cys-RIPK1 is an N-end rule substrate.
Mm **TRAF1**	152 DLEVD↓**C**YRA...A 409	Nd^t	Proapoptotic fragment, generated by caspase-8, of TRAF1, a regulator of apoptosis. Cys-TRAF1 is an N-end rule substrate.
Mm **BRCA1**	1118 DDLLD↓**D**VEI...D 1812	Nd^s	Proapoptotic fragment, generated by caspase-3, of the tumor suppressor BRCA1. Asp-BRCA1 is an N-end rule substrate.
Hs **LIMK1**	236 LDEID↓**L**LIQ...D 647	Nd^p	Proapoptotic fragment, generated by caspase-3, of LIMK1, a Ser/Thr protein kinase. Leu-LIMK1 is an N-end rule substrate.
Hs **NEDD9**	626 MDDYD↓**Y**VHL...F 834	Nd^p	Proapoptotic fragment, generated by caspase-3, of NEDD9, a regulator of cell adhesion. Tyr-NEDD9 is an N-end rule substrate.
Hs-**BID**	66 HSRLG↓**R**IEA...D 195	Nd^p	Proapoptotic fragment, generated by calpains, of BID, a regulator of apoptosis. Arg-BID is an N-end rule substrate.
Mm **BCL_{XL}**	56 SWHLA↓**D**SPA...K 233	Nd^s	Proapoptotic fragment, generated by calpains, of the antiapoptotic regulator BCL_{XL}. Asp-BCL_{XL} is an N-end rule substrate.
Mm **BIM_{EL}**	9 SSECD↓**R**EGG...H 196	Nd^p	Proapoptotic fragment, generated by caspase-3, of the apoptosis regulator BIM_{EL}. Arg-BIM_{EL} is an N-end rule substrate.
Mm **EPHA4**	769 RVLED↓**D**PEA...V 986	Nd^s	Proapoptotic fragment, generated by caspase-3, of the dependence receptor EPHA4. Cys-EPHA4 is an N-end rule substrate.
Mm **MET**	996 NESVD↓**Y**RAT...S 1379	Nd^p	Proapoptotic fragment, generated by caspase-3, of the dependence receptor MET. Tyr-MET is an N-end rule substrate.
Proapoptotic protein fragments that remain to be verified as N-end rule substrates			
Hs **PKCδ**	325 EDMQD↓**N**SGT...D 676	Nd^t	Proapoptotic fragment, generated by caspase-3, of the antiapoptotic protein kinase Cδ. Asn-PKCδ is a likely N-end rule substrate.
Hs **PKCθ**	350 LDEVD↓**K**MCH...S 706	Nd^p	Proapoptotic fragment, generated by caspase-3, of the antiapoptotic protein kinase Cθ. Lys-PKCθ is a likely N-end rule substrate.
Hs **ETK**	236 EDFPD↓**W**WQV...H 675	Nd^p	Proapoptotic fragment, generated by caspase-3, of the antiapoptotic ETK/BMX tyrosine kinase. Trp-ETK is a likely N-end rule substrate.
Mm **SLK**	432 PDTQD↓**Q**QTV...S 1202	Nd^t	Proapoptotic fragment, generated by caspase-3, of the SLK kinase, a regulator of actin. Gln-SLK is a likely N-end rule substrate.
Hs **HPK1**	381 YDDVD↓**I**PTP...L 833	Nd^p	Proapoptotic fragment, generated by caspase-3, of the Ser/Thr kinase HPK1. Ile-HPK1 is a likely N-end rule substrate.
Hs-**MLH1**	414 EDKTD↓**I**ISS...C 756	Nd^p	Proapoptotic fragment, generated by caspase-3, of the mismatch repair protein MLH1. Ile-MLH1 is a likely N-end rule substrate.

Fig. S1. Proapoptotic protein fragments that are experimentally confirmed substrates of the Arg/N-end rule pathway and fragments that remain to be verified as such. The name of a protein on the left is preceded by the acronym of a species (*Hs*, *Homo sapiens*; *Mm*, *Mus musculus*). As in the text, the names of proteins are in all capital letters for both human and mouse proteins. Amino acid residues are indicated by single-letter abbreviations. Arrowheads and the enlarged residue names in red indicate P1′ residues of the cleavage sites (i.e., the N-terminal residues of C-terminal fragments of the cleaved full-length proteins). Primary, secondary, and tertiary destabilizing N-terminal residues are denoted as Nd^p, Nd^s, and Nd^t, respectively (Fig. 1*A*) (1, 2). If a depicted cleavage site is one recognized by a caspase (the exceptions, in the present list, are the cleavage sites that yield Asp-BCL_{XL} and Arg-Bid, which are produced by calpains), the site is underlined. The residue number on the left is of the first shown residue of uncleaved protein numbered as in a full-length protein. The number on the right is of the last residue of a full-length protein. The first section of this figure describes 10 previously identified proapoptotic protein fragments, specifically Cys-RIPK1, Cys-TRAF1, Asp-BRCA1, Leu-LIMK1, Tyr-NEDD9, Arg-BID, Asp-BCL_{XL}, Arg-BIM_{EL}, Asp-EPHA4, and Tyr-MET. They were examined in the present study and found to be short-lived substrates of the Arg/N-end rule pathway (Figs. 2–4). Descriptions of these confirmed N-end rule substrates are in *SI Results, section I*. The second section describes six other previously identified proapoptotic fragments (all of them are produced by caspases) bearing destabilizing N-terminal residues that can be recognized by the Arg/N-end rule pathway. These fragments are likely N-end rule substrates but remain to be verified as such. Asn-PKCδ is the C-terminal fragment of the protein kinase Cδ (PKCδ) that can be generated by (in particular) caspase-3. This fragment bears N-terminal Asn (an Nd^t residue; see above for notations of destabilizing N-terminal residues) and is proapoptotic, in contrast to the full-length PKCδ kinase (3–7). Lys-PKCθ is the C-terminal fragment of the protein kinase Cθ (PKCθ). This fragment can be generated by (in particular) caspase-3, bears N-terminal Lys (an Nd^p residue), and is proapoptotic, in contrast to the full-length PKCθ kinase (8). Trp-ETK is the C-terminal fragment of the ETK/BMC tyrosine kinase, a member of the Btk/Tek family of kinases, at least some of which regulate apoptosis. The Trp-ETK fragment can be generated by (in particular) caspase-3, bears N-terminal Trp (an Nd^p residue), and is proapoptotic, in contrast to the full-length ETK kinase (9). Gln-SLK is the C-terminal fragment of SLK, an STE20-related protein kinase that plays a role in regulation of actin fibers. The Gln-SLK fragment can be generated by (in particular) caspase-3, bears N-terminal Gln (an Nd^t residue), and is proapoptotic. The concomitantly produced N-terminal fragment of SLK is also proapoptotic (10). Ile–hematopoietic progenitor kinase 1 (HPK1) is the C-terminal fragment of HPK1, an STE20-related protein kinase with functions that include stimulation of the stress-activated protein kinases SAPKs/JNKs and the NF-κB transcriptional regulon. The Ile-HPK1 fragment can be generated by (in particular) caspase-3, bears N-terminal Ile (an Nd^p residue), and is proapoptotic, in contrast to the full-length HPK1 kinase (11). Ile-MLH1 is the C-terminal fragment of the mismatch repair MLH1 protein that can be generated by (in particular) caspase-3, bears N-terminal Ile (an Nd^p residue) resides in the cytosol (unlike the full-length nuclear MLH1), and is proapoptotic, in contrast to full-length MLH1 (12).

1. Varshavsky A (2011) The N-end rule pathway and regulation by proteolysis. *Protein Sci* 20:1298–1345.
2. Sriram SM, Kim BY, Kwon YT (2011) The N-end rule pathway: Emerging functions and molecular principles of substrate recognition. *Nat Rev Mol Cell Biol* 12:735–747.
3. Emoto Y, Kisaki H, Manome Y, Kharbanda S, Kufe D (1996) Activation of protein kinase Cdelta in human myeloid leukemia cells treated with 1-beta-D-arabinofuranosylcytosine. *Blood* 87:1990–1996.
4. Denning MF, Wang Y, Nickoloff BJ, Wrone-Smith T (1998) Protein kinase Cdelta is activated by caspase-dependent proteolysis during ultraviolet radiation-induced apoptosis of human keratinocytes. *J Biol Chem* 273:29995–30002.

5. Leverrier S, Vallentin A, Joubert D (2002) Positive feedback of protein kinase C proteolytic activation during apoptosis. *Biochem J* 368:905–913.
6. Reyland ME (2007) Protein kinase Cdelta and apoptosis. *Biochem Soc Trans* 35:1001–1004.
7. LaGory EL, Sitailo LA, Denning MF (2010) The protein kinase Cdelta catalytic fragment is critical for maintenance of the G2/M DNA damage checkpoint. *J Biol Chem* 285:1879–1887.
8. Datta R, Kojima H, Yoshida K, Kufe D (1997) Caspase-3-mediated cleavage of protein kinase C theta in induction of apoptosis. *J Biol Chem* 272:20317–20320.
9. Wu YM, Huang CL, Kung HJ, Huang CYF (2001) Proteolytic activation of ETK/Bmx tyrosine kinase by caspases. *J Biol Chem* 276:17672–17678.
10. Sabourin LA, Tamai K, Seale P, Wagner J, Rudnicki MA (2000) Caspase 3 cleavage of the Ste20-related kinase SLK releases and activates an apoptosis-inducing kinase domain and an actin-disassembling region. *Mol Cell Biol* 20:684–696.
11. Arnold R, Liou J, Drexler HCA, Weiss A, Kiefer F (2001) Caspase-mediated cleavage of hematopoietic progenitor kinase 1 (HPK1) converts an activator of NFkappaB into an inhibitor of NFkappaB. *J Biol Chem* 276:14675–14684.
12. Chen F, Arseven OK, Cryns VL (2004) Proteolysis of the mismatch repair protein MLH1 by caspase-3 promotes DNA damage-induced apoptosis. *J Biol Chem* 279:27542–27548.

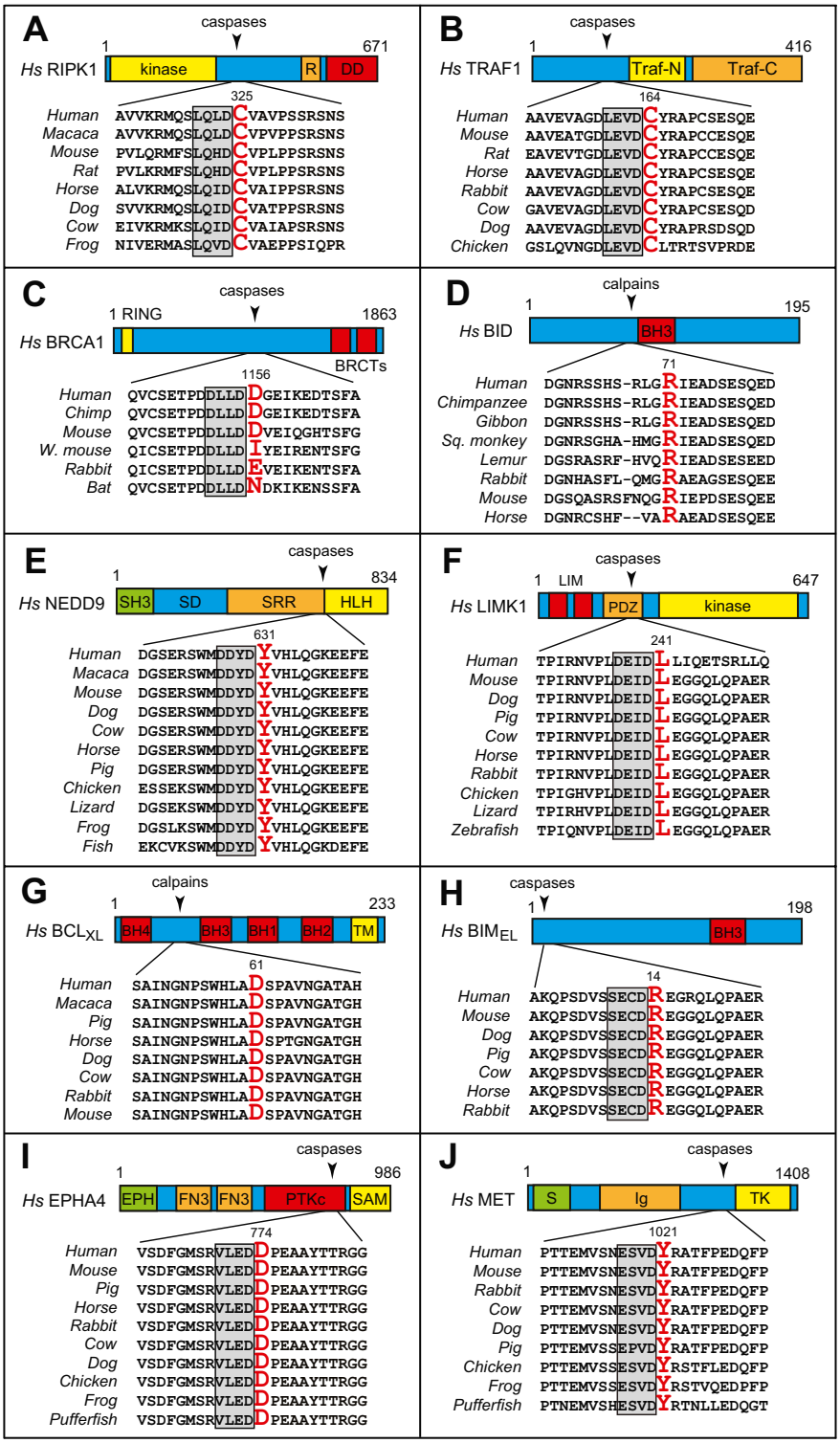

Fig. S2. Evolutionary conservation of the cleavage sites and destabilizing P1′ residues in the proapoptotic protein fragments Cys-RIPK1 (*A*), Cys-TRAF1 (*B*), Asp-BRCA1 (*C*), Leu-BID (*D*), Tyr-NEDD9 (*E*), Leu-LIMK1 (*F*), Asp-BCL_{XL} (*G*), Arg-BIM_{EL} (*H*), Asp-EPHA4 (*I*), and Tyr-MET (*J*). These fragments have been shown, in the present work, to be short-lived N-end rule substrates (Figs. 2 and 3). Except for Arg-BID and Asp-BCL_{XL} ((which are produced from full-length BID by calpains), these proapoptotic fragments are generated by caspases. Caspase cleavage sites are framed by rectangles and indicated by arrowheads. The indicated residue numbers, including the numbers of P1′ residues (shown in red), are of the human versions of the cited proteins. Approximate locations and names of specific protein domains are indicated as well. These fragments are described in *SI Results*, *section I*.

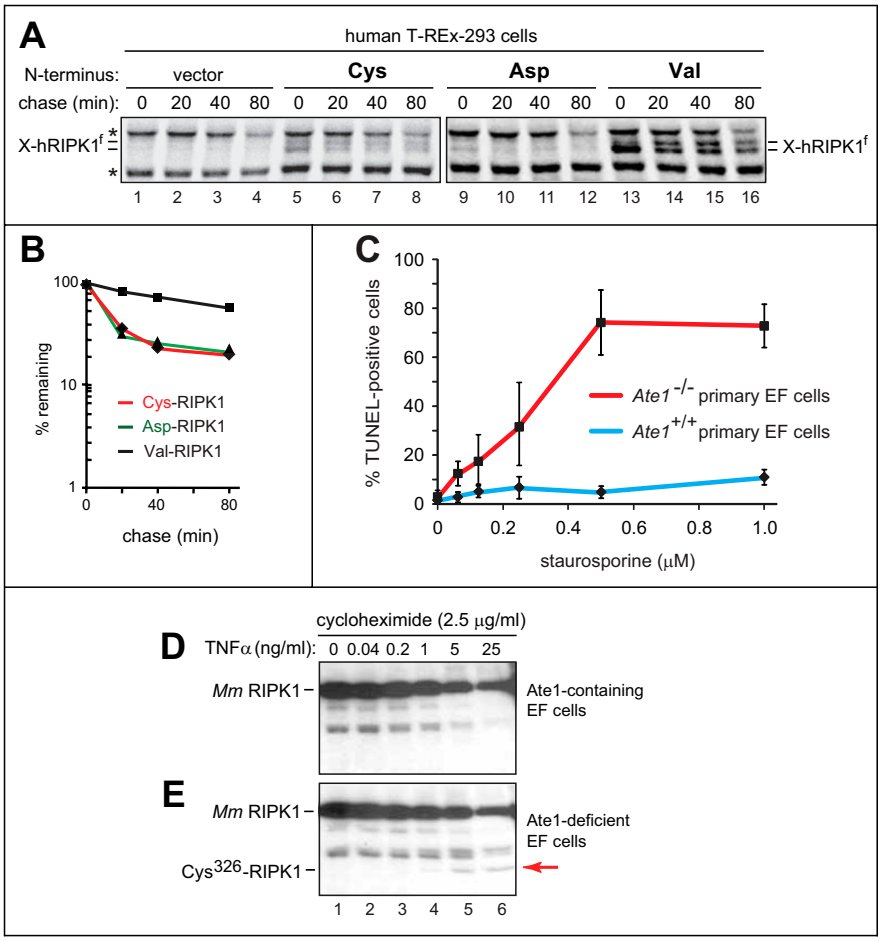

Fig. S3. In vivo degradation of X-RIPK1 fragments and apoptosis hypersensitivity of *Ate1*$^{-/-}$ cells. (*A*) ^{35}S–pulse-chase assays with human T-Rex-293–based cell lines that stably expressed human X^{325}-RIPK1^{f} proteins (*x* = Cys, Asp, Val) produced from the corresponding Ub-X^{325}-RIPK1^{f} fusions (1, 2). Expression of X-RIPK1^{f} was induced by Dox (0.1 μg/mL for 24 h). Cells were labeled at 37 °C for 10 min with [^{35}S]methionine/cysteine followed by a chase for 20, 40, and 80 min, immunoprecipitation of cell extracts with a monoclonal antibody to a C-terminal region of RIPK1, SDS/PAGE, autoradiography, and quantification (*SI Materials and Methods*). Lanes 1–4 show cells with integrated vector alone (negative control). **Proteins that cross-reacted with anti-RIPK1 antibody. Lanes 5–8 show Cys-RIPK1^{f}. Lanes 9–12 show Asp-RIPK1^{f}. Lanes 13–16 show Val-RIPK1^{f}. Of the two closely spaced bands of X-RIPK1^{f} in T-Rex-293 cells, the faster-migrating one was predominant immediately after the pulse, suggesting that the upper band of X-RIPK1^{f} was a modified (e.g., phosphorylated) derivative of the slower migrating species. (*B*) Quantification of data in *A*. ◆, Cys-RIPK1; ▲, Asp-RIPK1; ■, Val-RIPK1. In this quantification, the zero-point levels of each of the X-RIPK1 proteins were normalized to 100%. Note that this way of plotting the data omits the additional evidence for metabolic instability of Cys-RIPK1 and Asp-RIPK1 compared with Val-RIPK1. Specifically, the absolute levels of labeled Val-RIPK1 (*A*, lanes 13–16) were considerably higher compared with the levels of labeled Cys-RIPK1 and Asp-RIPK1 (lanes 5–12), reflecting a significant degradation of Cys-RIPK1 and Asp-RIPK1 before chase (during pulse) in contrast to Val-RIPK1. (*C*) Induction of apoptosis by staurosporine in primary (precrisis) WT (◆) and *Ate1*$^{-/-}$ (■) mouse EF cells. Cultures of primary EFs, derived from either WT or *Ate1*$^{-/-}$ mouse E13.5 embryos (3), were treated with increasing concentrations of staurosporine for 24 h followed by TUNEL measurements of the frequency of apoptotic cells. SDs are indicated (*SI Materials and Methods*). (*D* and *E*) ATE1-containing (*Ate1*$^{flox/-}$) mouse primary EF cells were treated either with (*D*) DMSO (the solvent for tamoxifen) alone or (*E*) tamoxifen in DMSO (50 ng/mL) for 5 d to transiently activate the Cre recombinase in tamoxifen-treated cells, thereby deleting the remaining copy of *Ate1* in these cells (4). Both (*D*) control (*Ate1*$^{flox/-}$) and (*E*) experimental (*Ate1*$^{-/-}$) cell cultures were grown for another 7 d before treatments for 24 h with increasing concentrations of TNFα in DMEM that also contained 0.5% FBS and a nontoxic (2.5 μg/mL) concentration of cycloheximide followed by SDS/PAGE of cell extracts and immunoblotting with a monoclonal antibody to a C-terminal region of RIPK1. At 5 ng/mL and higher concentrations of TNFα, ATE1-deficient apoptotic EF cells but not ATE1-containing cells contained readily detectable levels of a RIPK1 fragment that migrated at the M$_r$ of the 41-kDa Cys^{326}-RIPK1 fragment (red arrow).

1. Varshavsky A (2005) Ubiquitin fusion technique and related methods. *Methods Enzymol* 399:777–799.
2. Varshavsky A (2011) The N-end rule pathway and regulation by proteolysis. *Protein Sci* 20:1298–1345.
3. Kwon YT, et al. (2002) An essential role of N-terminal arginylation in cardiovascular development. *Science* 297:96–99.
4. Brower CS, Varshavsky A (2009) Ablation of arginylation in the mouse N-end rule pathway: Loss of fat, higher metabolic rate, damaged spermatogenesis, and neurological perturbations. *PLoS One* 4:e7757.

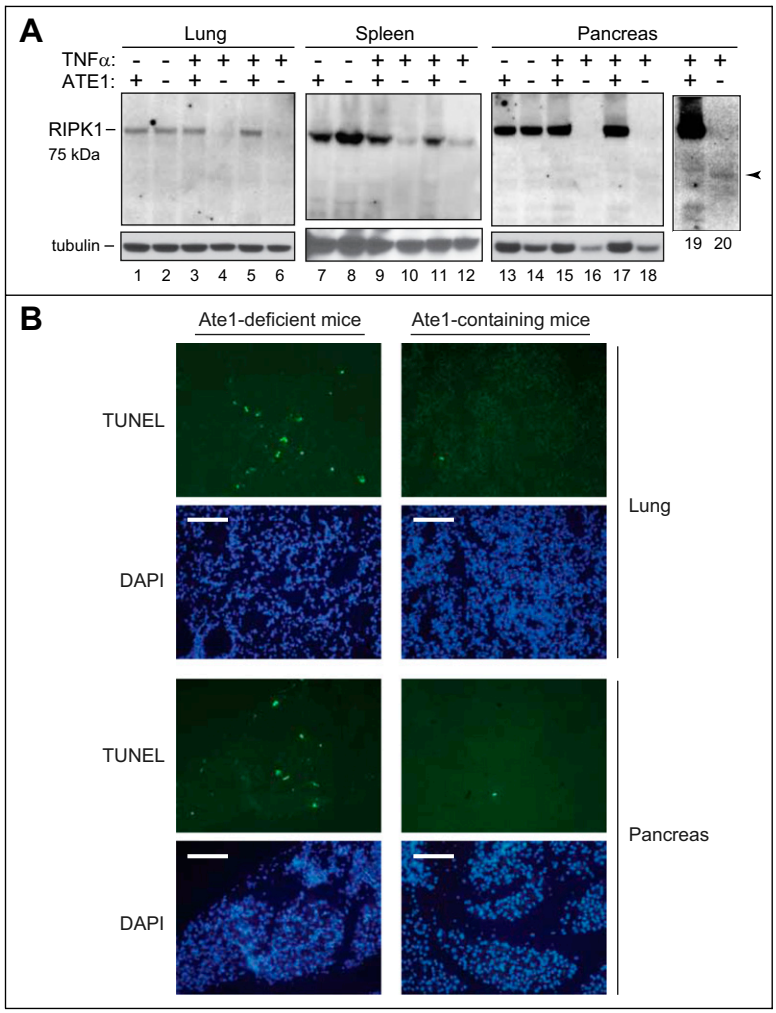

Fig. S4. Effects of TNFα on the levels of RIPK1 in ATE1-containing and -deficient mice and apoptosis hypersensitivity of ATE1-deficient mouse tissues; 3 wk after tamoxifen-mediated induction of Cre recombinase to ablate the remaining functional copy of the *Ate1* gene in *Ate1*$^{flox/-}$ mice (1), TNFα (50 μg/kg) was administered by tail vein injection. Control mice were injected with buffer alone. After 12 h, the indicated mouse tissues were harvested, and proteins in tissue extracts were analyzed by SDS/PAGE and immunoblotting with a monoclonal antibody to a C-terminal region of RIPK1, and also an antibody to β-tubulin (loading control). (*A*) Anti-RIPK1 immunoblots of proteins from lungs, spleens, and pancreases of three separate ATE1-containing and three separate ATE1-deficient mice that were either untreated or treated with TNFα (each lane corresponds to a sample from an individual mouse). Note the virtual disappearance of full-length RIPK1 from lungs and pancreases of TNFα-treated ATE1-deficient mice (in contrast to ATE1-containing mice) and a similar but less striking pattern in spleens. Note also a significant decrease of the relative tubulin content in samples from pancreases (but not in samples from lungs or spleens) of TNFα-treated ATE1-deficient mice, in contrast to ATE1-containing mice. These tubulin patterns were consistent with cytological signs of damage to acinar pancreatic cells of TNFα-treated ATE1-deficient (but not ATE1-containing) mice, and they were in agreement with the observed toxicity of TNFα to ATE1-deficient mice. Lanes 19 and 20, same as lanes 17 and 18, respectively, but a longer immunoblotting exposure that revealed a RIPK1 fragment (indicated by the arrowhead) that migrated at the M_r of the 41-kDa Cys^{326}-RIPK1 fragment (in the text). (*B*) ATE1-deficient mouse organs are hypersensitive to apoptosis. Representative images of 10-μm sections of lungs and pancreases from ATE1-containing and -deficient mice (1) that were treated for 12 h with TNFα. The sections were processed using the fluorescein-based TUNEL assay for apoptotic cells and staining with DAPI to visualize cell nuclei. (Scale bars, 100 μm.) *A* shows immunoblotting analyses of RIPK1 and Fig. 1*E* shows quantification of these data.

1. Brower CS, Varshavsky A (2009) Ablation of arginylation in the mouse N-end rule pathway: Loss of fat, higher metabolic rate, damaged spermatogenesis, and neurological perturbations. *PLoS One* 4:e7757.

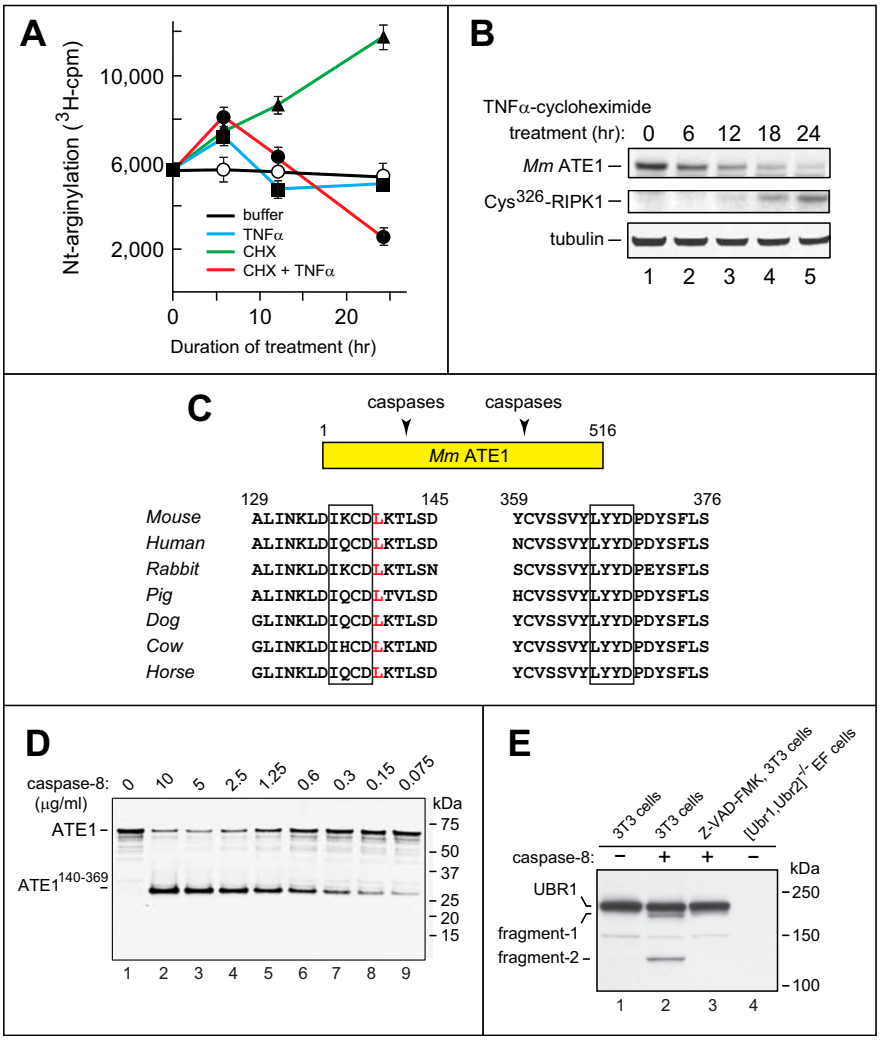

Fig. S5. Nt-arginylation under condition of apoptosis induction and caspase-mediated cleavages of ATE1 and UBR1. (*A*) In vitro Nt-arginylation assay with extracts from mouse NIH-3T3 cells supplemented, in particular, with Glu-lactalbumin (Nt-arginylation reporter) and L-^{3}H-arginine. Cells were treated as described below, followed by measurements of Nt-arginylation activity in cell extracts. ○, treatment with buffer alone; ■, TNFα (50 ng/mL); ▲, cycloheximide (10 μg/mL); ●, TNFα (50 ng/mL) and cycloheximide (10 μg/mL) together. (*B*) Extracts from 3T3 cells treated with TNFα and cycloheximide as described in *A* were fractionated by SDS/PAGE followed by immunoblotting with affinity-purified antibody to mouse ATE1, a monoclonal antibody to a C-terminal region RIPK1, and antibody to tubulin. (*C*) The mouse ATE1 R-transferase and the evolutionary conservation of its putative caspase-8/caspase-3 cleavage sites are framed by rectangles and indicated by arrowheads. A conserved destabilizing P1′ residue (Leu) at one of the cleavage sites is marked in red. The residue numbers shown are for the Ate1^{1B7A} isoform (1, 2). Both the 200-kDa mouse UBR1 E3 N-recognin and other E3 N-recognins (UBR2, UBR4, and UBR5) (Fig. 1*A*) also contain putative caspase-8/caspase-3 cleavage sites. (*D*) N-terminally His$_{10}$-tagged mouse Ate1^{1B7A} was expressed in *E. coli* and purified by Ni^{2+} affinity chromatography; 1 μg ATE1 was incubated in caspase assay buffer in a total volume of 20 μL either in the absence of added caspase-8 (lane 1) or with the indicated (decreasing) amounts of the recombinant human caspase-8 (lanes 2–8), followed by SDS/PAGE and immunoblotting with affinity-purified anti-ATE1 antibody. Fig. 4*B* shows direct evidence that caspase-8 can functionally inactivate the ATE1 R-transferase. (*E*) Extracts from mouse NIH 3T3 cells (lanes 1–3) or *Ubr1*$^{-/-}$ *Ubr2*$^{-/-}$ double-mutant mouse EF cells (2–4) that lacked the UBR1 and UBR2 N-recognins (lane 4; a control for specificity of anti-UBR1 antibody) were incubated in either (lanes 1 and 4) absence of added caspase-8 or (lanes 2 and 3) with recombinant caspase-8 (10 μg/mL), followed by SDS/PAGE and immunoblotting with antibody to mouse UBR1 (5). Z-VAD-FMK, a pan-caspase inhibitor, was added to the assay of lane 3. Two caspase-produced UBR1 fragments, the ∼180-kDa fragment-1 and the ∼130-kDa fragment-2, are indicated.

1. Hu R-G, et al. (2006) Arginyltransferase, its specificity, putative substrates, bidirectional promoter, and splicing-derived isoforms. *J Biol Chem* 281:32559–32573.
2. Varshavsky A (2011) The N-end rule pathway and regulation by proteolysis. *Protein Sci* 20:1298–1345.
3. Tasaki T, et al. (2005) A family of mammalian E3 ubiquitin ligases that contain the UBR box motif and recognize N-degrons. *Mol Cell Biol* 25:7120–7136.
4. An JY, et al. (2006) Impaired neurogenesis and cardiovascular development in mice lacking the E3 ubiquitin ligases UBR1 and UBR2 of the N-end rule pathway. *Proc Natl Acad Sci USA* 103:6212–6217.
5. Kwon YT, Xia Z, Davydov IV, Lecker SH, Varshavsky A (2001) Construction and analysis of mouse strains lacking the ubiquitin ligase UBR1 (E3alpha) of the N-end rule pathway. *Mol Cell Biol* 21:8007–8021.

Table S1. Plasmids used in this study

Plasmid	Description	Source or reference
pcDNA3.1-Neo	Amp^R; Neo^R; Expression vector for cloning your gene of interest	Invitrogen
pcDNA5/FRT/TO	Amp^R; Tetracycline inducible expression vector for cloning your gene of interest	Invitrogen
pOG44	Amp^R; Vector for transient expression of the Flp recombinase	Invitrogen
IMAGE clone: 30748947	Amp^R; full-length mouse TRAF1 cDNA	Open Biosystems
IMAGE clone: 6512978	Amp^R; full-length mouse EPHA4 cDNA	Open Biosystems
IMAGE clone: 40098362	Amp^R; 3′ fragment of mouse MET cDNA	Open Biosystems
Clone: LIFESEQ95191844	Amp^R; full-length human LIMK1 cDNA	Open Biosystems
Clone: 6830063	Amp^R; full-length mouse BCL_{XL} cDNA	Open Biosystems
Clone: 4459720	Amp^R; mouse BIM_{EL} cDNA	Open Biosystems
Clone: 30431022	Amp^R; full-length mouse mBRCA1 cDNA	Open Biosystems
Clone: 5179075	Amp^R; full-length human BID cDNA	Open Biosystems
Clone: 6299616	Cm^R; human NEDD9 cDNA	Open Biosystems
pKP378	Amp^R; Neo^R; pcDNA3.0-based plasmid encoding full-length mTRAF1-flag under the control of CMV promoter	This study
pKP379	Amp^R; Neo^R; pcDNA3.0-based plasmid encoding full-length mTRAF1 (D156A)-flag under the control of CMV promoter	This study
pKP380	Amp^R; Neo^R; pcDNA3.0-based plasmid encoding flag-Ub-Cys^{157}-mTRAF1-flag under the control of CMV promoter	This study
pKP381	Amp^R; Neo^R; pcDNA3.0-based plasmid encoding flag-Ub-Met^{157}-mTRAF1-flag under the control of CMV promoter	This study
pKP382	Amp^R; Neo^R; pcDNA3.0-based plasmid encoding flag-Ub-Asp^{157}-mTRAF1-flag under the control of CMV promoter	This study
pKP393	Amp^R; Neo^R; pcDNA3.0-based plasmid encoding full-length mRIPK1-ha_2 under the control of CMV promoter	This study
pKP394	Amp^R; Neo^R; pcDNA3.0-based plasmid encoding full-length hRIPK1-ha_2 under the control of CMV promoter	This study
pKP395	Amp^R; Neo^R; pcDNA3.0-based plasmid encoding flag-DHFR-ha-Ub-Cys^{326}-mRIPK1-ha_2-flag under the control of CMV promoter	This study
pKP396	Amp^R; Neo^R; pcDNA3.0-based plasmid encoding flag-DHFR-ha Ub-Asp^{326}-mRIPK1-ha_2-flag under the control of CMV promoter	This study
pKP397	Amp^R; Neo^R; pcDNA3.0-based plasmid encoding flag-DHFR-ha-Ub-Val^{326}-mRIPK1-ha_2-flag under the control of CMV promoter	This study
pKP399	Amp^R; Neo^R; pcDNA3.0-based plasmid encoding flag-DHFR-ha-Ub-Cys^{325}-hRIPK1-ha_2-flag under the control of CMV promoter	This study
pKP400	Amp^R; Neo^R; pcDNA3.0-based plasmid encoding flag-DHFR-ha-Ub-Asp^{325}-hRIPK1-ha_2-flag under the control of CMV promoter	This study
pKP401	Amp^R; Neo^R; pcDNA3.0-based plasmid encoding flag-DHFR-ha-Ub-Val^{325}-hRIPK1-ha_2-flag under the control of CMV promoter	This study
pKP409	Amp^R, Ura3; p416-Met25-based plasmid encoding flag-DHFR-Ub-Asp^{326}-mRIPK1-ha_2-flag under the control of Met25 promoter	This study
pKP411	Amp^R, Ura3; p416-Met25-based plasmid encoding flag-DHFR-Ub-Val^{326}-mRIPK1-ha_2-flag under the control of Met25 promoter	This study
pKP418	Amp^R; Hyg^R; pcDNA5/FRT/TO-based plasmid encoding Ub-Cys^{325}-hRIPK1-ha_2-flag under the control of Tet promoter	This study
pKP419	Amp^R; Hyg^R; pcDNA5/FRT/TO-based plasmid encoding Ub-Asp^{325}-hRIPK1-ha_2-flag under the control of Tet promoter	This study
pKP420	Amp^R; Hyg^R; pcDNA5/FRT/TO-based plasmid encoding Ub-Val^{325}-hRIPK1- ha_2-flag under the control of Tet promoter	This study
pKP492	Amp^R; Neo^R; pcDNA3.0-based plasmid encoding flag-DHFR-ha-Ub-Asp^{774}-mEPHA4-flag under the control of CMV promoter	This study
pKP493	Amp^R; Neo^R; pcDNA3.0-based plasmid encoding flag-DHFR-ha Ub-Val^{774}-mEPHA4-flag under the control of CMV promoter	This study
pKP496	Amp^R; Neo^R; pcDNA3.0-based plasmid encoding flag-DHFR-ha Ub-MCS-flag under the control of CMV promoter; MCS has SacII, EcoRI, XhoI, ClaI, and EcoRV unique cloning sites	This study
pKP512	Amp^R; Neo^R; pcDNA3.0-based plasmid encoding flag-DHFR-ha Ub-Leu^{241}-hLIMK1-flag under the control of CMV promoter	This study
pKP513	Amp^R; Neo^R; pcDNA3.0-based plasmid encoding flag-DHFR-ha Ub-Val^{241}-hLIMK1-flag under the control of CMV promoter	This study
pKP514	Amp^R; Neo^R; pcDNA3.0-based plasmid encoding flag-DHFR-ha Ub-Asp^{61}-mBCL_{XL}-flag under the control of CMV promoter	This study
pKP515	Amp^R; Neo^R; pcDNA3.0-based plasmid encoding flag-DHFR-ha Ub-Val^{61}-mBCL_{XL}-flag under the control of CMV promoter	This study

Table S1. Cont.

Plasmid	Description	Source or reference
pKP519	Amp^R; Neo^R; pcDNA3.0-based plasmid encoding flag-DHFR-ha Ub-Tyr^{1001}-mMET-flag under the control of CMV promoter	This study
pKP520	Amp^R; Neo^R; pcDNA3.0-based plasmid encoding flag-DHFR-ha Ub-Val^{1001}-mMET-flag under the control of CMV promoter	This study
pKP521	Amp^R; Neo^R; pcDNA3.0-based plasmid encoding flag-DHFR-ha Ub-Arg^{14}-mBIM_{EL}-flag under the control of CMV promoter	This study
pKP522	Amp^R; Neo^R; pcDNA3.0-based plasmid encoding flag-DHFR-ha Ub-Val^{14}-mBIM_{EL}-flag under the control of CMV promoter	This study
pKP523	Amp^R; Neo^R; pcDNA3.0-based plasmid encoding flag-DHFR-ha Ub-Arg^{71}-hBID-flag under the control of CMV promoter	This study
pKP524	Amp^R; Neo^R; pcDNA3.0-based plasmid encoding flag-DHFR-ha Ub-Val^{71}-hBID-flag under the control of CMV promoter	This study
pKP526	Amp^R; Neo^R; pcDNA3.0-based plasmid encoding flag-DHFR-ha Ub-Tyr^{631}-Hnedd9-flag under the control of CMV promoter	This study
pKP527	Amp^R; Neo^R; pcDNA3.0-based plasmid encoding flag-DHFR-ha Ub-Val^{631}-hNEDD9-flag under the control of CMV promoter	This study
pKP528	Amp^R; Neo^R; pcDNA3.0-based plasmid encoding flag-DHFR-ha Ub-Asp^{1119}-mBRCA1-flag under the control of CMV promoter	This study
pKP529	Amp^R; Neo^R; pcDNA3.0-based plasmid encoding flag-DHFR-ha Ub-Val^{1119}-mBRCA1-flag under the control of CMV promoter	This study

Table S2. Primers used in this study

Primer	Primer's sequence
647	TTCTCGAGCTAGGCGTAATCTGGGACATCGTATGGGTAGGAACCTGAGGCGTAATCTGGG
650	AAATAAAGCTTATGCAACCAGACATGTCCTTGG
651	AACCTGAGGCGTAATCTGGGACATCGTAAGGGTAGCTCTGGCTGGCACGAATCA
652	TTTTTAAGCTTATGCAACCAGACATGTCCTTG
653	AACCTGAGGCGTAATCTGGGACATCGTAAGGGTAGTTCTGGCTGACGTAAATCAAGC
697	TTCTCGAGCTAACCTTTGTCGTCATCGTCTTTGTAGTCGGCGTAATCTGGGACATCGTAT
702	TTTTTCCCGGGTGTGTACCCTTACCTCCGAGCAG
703	TTTTTCCCGGGGACGTACCCTTACCTCCGAGCAG
705	TTTTTCCCGGGGTTGTACCCTTACCTCCGAGCAG
707	TTTTTCCCGGGTGTGTGGCAGTACCTTCAAGCC
708	TTTTTCCCGGGGACGTGGCAGTACCTTCAAGCC
709	TTTTTCCCGGGGTTGTGGCAGTACCTTCAAGCC
1,188	CACACGGATCCACCATGGCCTCCAGCTCAGCCCCT
1,189	TTTTTTCTAGATAACCTTTGTCGTCATCGTCTTTGTAGTCAGCACTAGTGTCCACAATGC
1,190	GACCTGGAGGTAGCCTGCTACCGGGC
1,191	GCCCGGTAGCAGGCTACCTCCAGGTC
1,193	CACACGGATCCACCATGAACATTTTCGTCAAGACTTTGACC
1,194	CCCGCCTCTTAGCCTTAGCACA
1,195	TGTGCTAAGGCTAAGAGGCGGGGACTACCGGGCACCTTGCTGT
1,196	TGTGCTAAGGCTAAGAGGCGGGGTTTACCGGGCACCTTGCTGT
1,197	CACACGGATCCACCATGGTTGACTACAAGGACGACGACGACAAGGGA
1,198	AAGGACGACGACGACAAGGGACAGATTTTCGTCAAGACTTTG
1,369	TATAGCCCGGGGACCCCGAAGCAGCCTACACTACC
1,370	TATAGCCCGGGGTTCCCGAAGCAGCCTACACTACC
1,371	TAATTTCTAGATTAACCTTTGTCGTCATCGTCTTTGTAGTCGACAGGAACCATCCTGCCA
1,447	GGGAATTCCTCGAGATCGATATCGACTACAAAGACGATGACGACAAAGGTTAAT
1,448	CTAGATTAACCTTTGTCGTCATCGTCTTTGTAGTCGATATCGATCTCGAGGAATTCCCGC
1,426	AAAAACCGCGGAGGATACAGAGCTACTTTTCCAGAAGACCAGT
1,427	AAAAACCGCGGAGGAGTTAGAGCTACTTTTCCAGAAGACCAGT
1,428	TTTGTATCGATTGTGTTCCCCTCGCCATCA
1,432	AAAAACCGCGGAGGAGATAGCCCGGCCGTGAATGGAGC
1,433	AAAAACCGCGGAGGAGTTAGCCCGGCCGTGAATGGAGC
1,434	TTTTAATCGATCTTCCGACTGAAGAGTGAGCCC
1,435	AAAAACCGCGGAGGAAGAGAAGGTGGACAATTGCAGCCTG
1,436	AAAAACCGCGGAGGAGTTGAAGGTGGACAATTGCAGCCTG
1,437	TTTTAATCGATATGCCTTCTCCATACCAGACGG
1,438	AAAACCGCGGAGGAGATGTTGAAATACAGGGACATACTAGCTT
1,439	AAAACCGCGGAGGAGTTGTTGAAATACAGGGACATACTAGCTT
1,440	TTTTAATCGATATCATTGGAGTCTTGTGGCTCAC
1,467	AAAAACCGCGGAGGACTGCTGATTCAGGAAACCAGCCG
1,468	AAAAACCGCGGAGGAGTTCTGATTCAGGAAACCAGCCG
1,469	TTTTAATCGATGTCGGGGACCTCAGGGTGGGC
1,473	AAAACCGCGGAGGAAGAATAGAGGCAGATTCTGAAAGTCAAG
1,474	AAAACCGCGGAGGAGTTATAGAGGCAGATTCTGAAAGTCAAG
1,475	TTTTAATCGATGTCCATCCCATTTCTGGCTAAGC
1,479	AAAAACCGCGGAGGATACGTCCACCTACAGGGTAAGGAGGAGT
1,480	AAAAACCGCGGAGGAGTTGTCCACCTACAGGGTAAGGAGGAGT
1,481	TTTTAATCGATGAACGTGGCCATCTCCAGCAAAGAG